



HAL
open science

Self-heating and trapping effects in AlGa_N/Ga_N heterojunction field-effect transistors

I. Saidi, M. Gassoumi, H. Maaref, H. Mejri, Christophe Gaquière

► **To cite this version:**

I. Saidi, M. Gassoumi, H. Maaref, H. Mejri, Christophe Gaquière. Self-heating and trapping effects in AlGa_N/Ga_N heterojunction field-effect transistors. *Journal of Applied Physics*, 2009, 106, pp.054511-1-7. 10.1063/1.3202317 . hal-00473632

HAL Id: hal-00473632

<https://hal.science/hal-00473632>

Submitted on 25 May 2022

HAL is a multi-disciplinary open access archive for the deposit and dissemination of scientific research documents, whether they are published or not. The documents may come from teaching and research institutions in France or abroad, or from public or private research centers.

L'archive ouverte pluridisciplinaire **HAL**, est destinée au dépôt et à la diffusion de documents scientifiques de niveau recherche, publiés ou non, émanant des établissements d'enseignement et de recherche français ou étrangers, des laboratoires publics ou privés.

Self-heating and trapping effects in AlGaN/GaN heterojunction field-effect transistors

Cite as: J. Appl. Phys. **106**, 054511 (2009); <https://doi.org/10.1063/1.3202317>

Submitted: 01 June 2009 • Accepted: 13 July 2009 • Published Online: 15 September 2009

I. Saidi, M. Gassoumi, H. Maaref, et al.



View Online



Export Citation

ARTICLES YOU MAY BE INTERESTED IN

Effect of self-heating on electrical characteristics of AlGaN/GaN HEMT on Si (111) substrate
AIP Advances **7**, 085015 (2017); <https://doi.org/10.1063/1.4990868>

Two dimensional electron gases induced by spontaneous and piezoelectric polarization in undoped and doped AlGaN/GaN heterostructures

Journal of Applied Physics **87**, 334 (2000); <https://doi.org/10.1063/1.371866>

Two-dimensional electron gases induced by spontaneous and piezoelectric polarization charges in N- and Ga-face AlGaN/GaN heterostructures

Journal of Applied Physics **85**, 3222 (1999); <https://doi.org/10.1063/1.369664>

Lock-in Amplifiers
up to 600 MHz



Zurich
Instruments



Self-heating and trapping effects in AlGaIn/GaN heterojunction field-effect transistors

I. Saidi,^{1,a)} M. Gassoumi,¹ H. Maaref,^{1,a)} H. Mejri,^{1,2} and C. Gaquière³

¹Laboratoire de Physique des Semiconducteurs et des Composants Electroniques, Département de Physique, Faculté des Sciences de Monastir, 5019 Monastir, Tunisia

²Unité de Recherche de Mathématiques Appliquées et Physique Mathématiques, Ecole Préparatoire aux Académies Militaires, Avenue Maréchal Tito, 4029 Sousse, Tunisia

³Institut d'Electronique de Microélectronique et de Nanotechnologie IEMN (TIGER), Département hyperfréquences et Semiconducteurs, Université des Sciences et Technologies de Lille, Avenue Poincaré, 59652 Villeneuve d'Ascq Cedex, France

(Received 1 June 2009; accepted 13 July 2009; published online 15 September 2009)

This work first attempted to simulate the band edges of AlGaIn/GaN high electron mobility transistors (HEMTs) structures with Ga-face polarity at the heterointerface. The spontaneous and piezoelectric-induced polarization fields as well as the effects of temperature on the electron band parameters have been included into the modeling. In a second step, we calculated self-consistently direct-current characteristics of AlGaIn/GaN HEMTs without considering any defect. Calculations were made as a function of doping concentration and Al composition. In the paper, the self-heating in AlGaIn/GaN HEMTs grown on SiC substrate before and after Si₃N₄ passivation was also investigated revealing that: (i) power dissipation is induced due to the increase in drain bias, which leads to a temperature rise of the two-dimensional electron gas in the channel, (ii) an enhancement in drain current is achieved after Si₃N₄ passivation, (iii) the self-heating occurs even in AlGaIn/GaN heterostructures after passivation. Including thermal and trapping effects in transistor device model can allow adjusting of some of the electron transport parameters in order to obtain optimized current at the output. © 2009 American Institute of Physics. [doi:10.1063/1.3202317]

I. INTRODUCTION

GaN, AlN, and their ternary alloys are very promising candidates for high power and high frequency applications,^{1–11} due to their wide band gap, high thermal stability, high electron velocity, and large breakdown electric field. AlGaIn/GaN heterostructures have recently been used to develop high electron mobility transistors (HEMTs) aimed at operating at high temperature.^{8–11} A peculiar feature of AlGaIn-based transistors with the wurtzite crystal structure is the formation of a two-dimensional electron gas (2DEG) at the AlGaIn/GaN heterointerface, due mainly to spontaneous and piezoelectric polarizations.^{11–20} Indeed, relatively high electron densities can be achieved in AlGaIn/GaN HEMTs without doping intentionally the barriers. In doped AlGaIn/GaN heterostructures, the crucial problem is how to achieve both a high electron transport and a high transconductance in a transistor device based on this system. Back doping^{21,22} has been suggested as a method to obtain high electron sheet concentrations in HEMTs with thin barrier epilayers. As was found, the use of this doping design led to an improvement in the electron transport.

However, applications of AlGaIn/GaN HEMTs are limited by the presence of defects. Among them, the electron trapping states at the active surface zone can induce a collapse in the drain-source current.²³ As a result of this device degradation, the output power considerably decreases and hot electrons are captured by deep traps, which lead to the

formation of a virtual gate at the vicinity of the channel.²⁴ A number of works has been undertaken to the subject of trapping effects by using different electrical characterization techniques.^{25–28} As is also found in AlGaIn/GaN HEMTs operating at large biases, the high-power dissipation induces a self-heating in the active layers. It results in an enhanced phonon scattering, which causes a decrease in the carrier mobility and in the electron saturation velocity as well. Evidence of the self-heating effect is the observation of a negative differential conductance in the drain-source current. In a HEMT device with small sizes and at relatively high current densities, the self-heating does not only limit the electron transport but also damages the gate. To overcome the self-heating, AlGaIn/GaN HFETs, and HEMTs have been pseudomorphically grown on sapphire, SiC, and bulk GaN as substrates.^{29–32} Comparison of the HFETs investigated favors transistors grown on SiC.³⁰ This is assigned to the higher thermal conductivity of SiC, which allows a better heat dissipation from the active zone. On the other hand, different designs have been used to tailor the electric field in order to reduce the effect of self-heating. However, reliability and performance remain subject of concern and interest. To further optimize device designs, measurement of local temperature throughout active region, particularly in the channel, is essential. Experimental works are being done to this end.^{33–36} As has been revealed from visible and ultraviolet micro-Raman scattering measurements,^{34,35} the self-heating within an operating AlGaIn/GaN HEMT shows a gradient parallel to the growth direction. More especially, the hot spot is found to be located at the edge of the gate electrode and the tem-

^{a)}Authors to whom correspondence should be addressed. Electronic addresses: saidiimenlps@yahoo.fr and hassen.maaref@fsm.rnu.tn.

perature rise can attain 240 K over ambient under aggressive functioning conditions. Theoretically, to obtain more accurate characteristics from device simulations, the effect of the self-heating has been considered.³⁷⁻⁴¹

The aim of the present work is to investigate the effects of self-heating on the transport properties of AlGaIn/GaN HEMTs. The subbands and their related envelope wave functions as well as the relation of sheet carrier concentration and the Fermi energy have been calculated self-consistently by taking into account the piezoelectric and spontaneous polarizations. This has been used to simulate the current-voltage (*I-V*) characteristics, by including the thermal effects. As an experimental support, we have taken direct current (dc) characteristics of AlGaIn/GaN HEMTs grown on SiC substrate measured at room temperature. From the relevant characteristics, we deduced the temperature rise of the 2DEG as a function of the drain bias for different gate voltages. We also studied the electron transport in the same HEMT structures after Si₃N₄ passivation. As a result, the current at the output is found to be increasing with Si₃N₄ passivation, while the self-heating remains to occur in passivated HEMT devices. The paper is organized as follows. After a brief introduction, we present, in Sec. II, the model formulation and results; conclusions derived from the study are summarized in the Sec. III.

II. THEORETICAL FORMULATION AND RESULTS

A. The band edges of AlGaIn/GaN HEMTs at zero bias

The heterostructure to model consists of an AlGaIn/GaN HEMT with Ga-face polarity, being assumed to be grown on a GaN underlayer. The existence of a large polarization field at the AlGaIn/GaN heterointerface gives rise to higher sheet-carrier concentrations that occur in the GaN channel. The bandgap edge of such a system can be simply computed if there are no defects apart from the donor atoms. Residual impurities are accounted as a uniform doping in the epilayers. The heterostructure is considered at a temperature *T* and no external electric field is applied at the output of the HEMT device. Taking into account the polarization effects, the total amount of polarization-induced sheet charge density for a top/bottom AlGaIn/GaN is given by¹⁹

$$\sigma = [P_{\text{PE}}(\text{GaN}) - P_{\text{PE}}(\text{AlGaIn})] + [P_{\text{SP}}(\text{GaN}) - P_{\text{SP}}(\text{AlGaIn})], \quad (1)$$

with

$$P_{\text{SP}}(\text{AlGaIn}) = -0.09x - 0.034(1-x) + 0.021x(1-x)$$

and

$$P_{\text{PE}}(\text{AlGaIn/GaN}) = -0.0525x + 0.0282x(1-x),$$

where *x* is the Al composition and *P*_{SP} and *P*_{PE} denote the spontaneous and piezoelectric polarizations, respectively. Regarding the dependence of these parameters on temperature, only the change in spontaneous polarization has been measured and is found to be small enough. Recent data give a change coefficient with temperature of this polarization, *dP*_{SP}/*dT*, of the order of 0.91×10^{-6} for GaN (Ref. 42) and 7.5×10^{-6} C K⁻¹ m⁻² for AlN.⁴² For Al_{*x*}Ga_{1-*x*}N, this coeffi-

cient can be assumed to vary linearly with the composition *x*. This correction in the polarization due to a variation in temperature is considered in our simulation. Another parameter that governs the improved electron transport in AlGaIn/GaN HEMTs is the 2DEG sheet carrier concentration. The amount of polarization-induced charge density being to the model as well as the total 2DEG concentration can be calculated from coupled Schrödinger and Poisson equations:

$$\left[-\frac{\hbar^2}{2} \frac{d}{dz} \frac{1}{m^*(z)} \frac{d}{dz} + V_B(z) + V_H(z) + V_{XC}(z) + V_P(z) - \varepsilon_\nu(k_z) \right] \phi_{\nu,k_z}(z) = 0 \quad (2)$$

and

$$\frac{\varepsilon_0}{e^2} \frac{d}{dz} \varepsilon_r(z) \frac{d}{dz} (V_H + V_P) = \frac{\sigma}{e} \delta(z - z_0) + N_D(z) - n(z), \quad (3)$$

where *z* is the growth direction, *m*^{*}(*z*) is the electron effective mass at the bottom of the Γ conduction band, ν is the subband index, *k*_{*z*} denotes the vector momentum parallel to the *z*-direction, $\varepsilon_0 \varepsilon_r(z)$ is the total dielectric constant of the host lattice, *z*₀ is the interface position, *V*_{*B*}(*z*) represents the barrier potential due to the heterojunction bandgap discontinuity, *V*_{*H*}(*z*) is the effective Hartree potential related to screened ionized donors, *V*_{*XC*}(*z*) is the exchange-correlation potential resulting from the many-body effects,⁴³ *V*_{*P*}(*z*) is the polarization charge-induced potential, and *N*_{*D*}(*z*) and *n*(*z*) are the total density of ionized donors and the sheet concentration of confined electrons, respectively. In evaluating the potential energy *V*_{*B*}(*z*), the AlGaIn/GaN heterointerface is assumed to be abrupt and the conduction-band offset is given in Ref. 42. It is to be noticed that the temperature dependence of the latter electron band parameter is included in the band gap of the Al_{*x*}Ga_{1-*x*}N material.⁴² The effective masses of electrons are taken as $0.2m_0$ and $0.48m_0$ for GaN and AlN, respectively,⁴⁴ where *m*₀ is the free electron mass. For AlGaIn, the electron effective mass is deduced using Vegard's law. The Al composition as well as the doping concentration in the AlGaIn barrier are treated as parameters. Figure 1 shows a diagram of the epitaxial layers piling and the energy-band profile for an AlGaIn/GaN HEMT with Ga face polarity. Calculation of the confining potential has been made for a doping density *N*_{*D*} = 10^{18} cm⁻³, a channel width *d*_{CH} = 31 nm, an Al composition *x* = 0.22, a thickness of the undoped AlGaIn spacer *d*_{*i*} = 3 nm, and a width of the doped AlGaIn layer *d*_{*j*} = 28 nm. The density of residual donors is taken as *N*_{*DR*} = 5×10^{16} cm⁻³ in both GaN and AlGaIn epilayers. In the energy-band diagram, the subband energies, the square of the eigenenvelope wave functions, and the Fermi level calculated at *T* = 300 K are reported. As also shown, the 2DEG is located at the lower AlGaIn/GaN interface in an asymmetric triangular potential well with only the ground and the first excited states *E*₁ and *E*₂ occupied. At this stage, we have not taken into account the presence of eventual defects such as those related to the surface states. Indeed, surface states, if present, consist of several kinds of defects having different ionization energies within the band gap. In an HEMT device, these defects can behave as trapping cen-

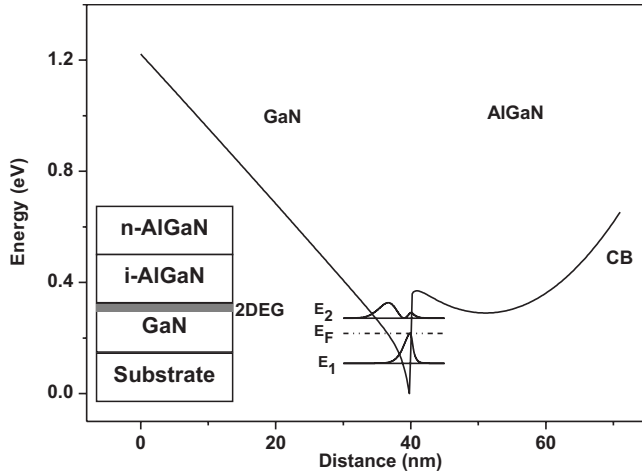


FIG. 1. The conduction-band edge calculated for an AlGaIn/GaN HEMT with Ga-face polarity. In the plots are also reported the subband energies, the envelope wave functions, and the Fermi level. The 2DEG is located at the lower AlGaIn/GaN interface, as schematically indicated in the inset.

ters thus leading to a reduction in the 2DEG density. Here, to simplify, the surface states are considered as a single species with adjustable sheet concentration and discrete ionization energy. They are also assumed to be ionized and their concentration is treated as a parameter. Let N_{SD} be the total area concentration of ionized surface donors, which should be included in the charge balance equation. We calculated the total density n_s of the 2DEG as a function of N_{SD} in the range $0-5 \times 10^{12} \text{ cm}^{-2}$. It has been found that the amount of confined electrons decreases from 1.26×10^{13} to $8.23 \times 10^{12} \text{ cm}^{-2}$ as N_{SD} increases. In the following, the density N_{SD} is fixed at $1 \times 10^{12} \text{ cm}^{-2}$.

B. Transport characteristics of ideal AlGaIn/GaN HEMT structures

As demonstrated above, the AlGaIn/GaN HEMT simulated shows only the first two subbands occupied at $T = 300 \text{ K}$. Thus, the total density of the 2DEG accumulated in the channel can be approximately expressed as

$$n_s = \frac{m^* k_B T}{\pi \hbar^2} \left[\log \left(1 + \exp \frac{E_F - E_1}{k_B T} \right) + \log \left(1 + \exp \frac{E_F - E_2}{k_B T} \right) \right], \quad (4)$$

where k_B and \hbar are the Boltzmann and Planck constants and E_F is the Fermi energy. The self-consistent solutions of the Schrödinger and Poisson equations give the subband energies E_1 and E_2 as a function of the Al composition x and the doping density N_D . On the other hand, the density of charge depleted in AlGaIn/GaN can be obtained using the assumption of total depletion according to the relation⁴⁵⁻⁴⁷

$$n_s = \frac{\varepsilon(x)}{ed} \left(V_{gs} - \frac{E_F}{e} - V_{th} \right), \quad (5)$$

with

$$V_{th} = \frac{E_b}{e} - \frac{\Delta E_c}{e} + \frac{e N_d}{2\varepsilon(x)} d_d^2 - \frac{\sigma d}{\varepsilon(x)},$$

where $\varepsilon(x)$ is the x -dependent dielectric constant of AlGaIn, d is the total thickness of the barrier layer, V_{gs} represents the applied gate bias, V_{th} is the threshold voltage, E_b denotes the Schottky barrier height, and ΔE_c is the conduction-band discontinuity at the AlGaIn/GaN heterointerface. Equations (4) and (5) have to be solved simultaneously and the interfacial sheet electron concentration is given by, for weak inversion,

$$n_s = n_{s0} \exp \left[\frac{e \varepsilon(x)}{\varepsilon(x) K_B T + n_{s0} e^2 d} \left(V_{gs} - V_{th} - \frac{n_0 e d}{\varepsilon(x)} \right) \right], \quad (6)$$

with

$$n_{s0} = \frac{m^* k_B T}{\pi \hbar^2} (e^{-E_1/K_B T} + e^{-E_2/K_B T}).$$

For strong inversion,

$$n_s = \frac{2m^* e^2 d}{(2e^2 d m^* + \varepsilon(x) \pi \hbar^2)} \left[(V_{gs} - V_{th}) \frac{\varepsilon(x)}{ed} + K \right] - K, \quad (7)$$

with

$$K = \frac{m^*}{\pi \hbar^2} (E_1 + E_2).$$

It is worth noticing that the Fermi level E_F lies at the bottom of the subbands E_1 and E_2 for weak inversion and shifts up in energy as the gate bias V_{gs} increases to achieve the strong inversion regime. As shown from Eqs. (6) and (7), the density of 2DEG is controlled by the bias voltage applied to the gate. The source-to-drain current is the sum of drift and diffusion currents and is expressed as follows:

$$I_{ds} = \frac{Ze \mu_0}{1 + \frac{1}{F_c} \frac{dV}{dy}} \left(n_s(y) \frac{dV}{dy} + \frac{K_B T}{e} \frac{dn_s(y)}{dy} \right), \quad (8)$$

where y is the distance along the channel from the source, μ_0 is the low-field mobility, F_c is the critical electric field, Z is the gate width, and $V(y)$ is the effective gate voltage at position y . In modeling of the low-field mobility, we included dislocation, ionized impurity, deformation potential acoustic phonon, piezoelectric, and polar optical phonon scattering contributions.⁴⁸⁻⁵¹ Under this form, the dependence of μ_0 on temperature is taken into account. The current I_{ds} in the different operating regimes can then be determined using the corresponding expressions for sheet carrier concentration with the gate voltage replaced by the effective gate bias $V_{gs} - V(y)$ at position y . Equation (8) is integrated along the channel length L with use of the boundary conditions: $V(y=0) = R_s I_{ds}$ and $V(y=L) = V_{ds} - (R_s + R_d) I_{ds}$, where R_s and R_d are the source and drain contact resistances and V_{ds} is the bias voltage applied to the drain with respect to the grounded source. Accordingly, the current-voltage characteristics can be derived from the following equations.

In weak inversion regime,

$$\begin{aligned} & \frac{(R_s + R_d)}{F_c} I_{ds}^2 - \left(L + \frac{V_{ds}}{F_c} \right) I_{ds} \\ & + \left(\frac{1}{\alpha} - \frac{k_B T}{e} \right) Z e \mu_0 n_{s0} \exp \alpha (V_{gs} - \beta) \\ & \times [\exp(-\alpha R_s I_{ds}) - \exp - \alpha (V_{ds} - R_d I_{ds})] = 0, \quad (9) \end{aligned}$$

with

$$\alpha = \frac{e \varepsilon(x)}{\varepsilon(x) k_B T + n_{s0} e^2 d}$$

and

$$\beta = V_{th} + \frac{n_{s0} e d}{\varepsilon(x)}.$$

For strong inversion,

$$\begin{aligned} & \left[\frac{R_s + R_d}{F_c} + a(R_s^2 - R_d^2) \right] I_{ds}^2 - \left[L + \frac{V_{ds}}{F_c} + b(R_s + R_d) \right. \\ & \left. - 2aR_d V_{ds} \right] I_{ds} - (aV_{ds} - b)V_{ds} = 0, \quad (10) \end{aligned}$$

with

$$a = \frac{\mu_0 Z e^2 m^* \varepsilon(x)}{2m^* e^2 d + \pi \varepsilon(x) \hbar^2}$$

and

$$b = \frac{2Z e^2 m^* \mu_0 \varepsilon(x)}{2m^* e^2 d + \pi \varepsilon(x) \hbar^2} \left(V_{gs} - \frac{k_B T}{e} - V_{th} - \frac{K \pi \hbar^2}{2m^* e} \right).$$

All of the parameters are defined above. Equations (9) and (10), coupled to those in Eqs. (2) and (3), give self-consistent solutions for the drain current in the AlGaIn/GaN HEMTs investigated. Using Eqs. (6) and (7), we calculated the sheet carrier concentration n_s as a function of the gate bias V_{gs} for various widths d_d of the doped AlGaIn layer. The results are depicted in Fig. 2(a). Calculations were carried out for $x = 0.22$, $N_D = 10^{18} \text{ cm}^{-3}$, and $T = 300 \text{ K}$. As shown from the plots, the 2DEG density increases with V_{gs} and d_d . Moreover, the threshold voltage shifts toward increasingly negative values with increased d_d . The reason for increased 2DEG sheet density is the following: with strong polarizations, the AlGaIn/GaN HEMTs with thick doped barriers require less drain biases to achieve a finite electron concentration. Figure 2(b) shows the 2DEG density n_s versus the gate voltage, calculated for different Al compositions. As can be seen, higher Al mole fractions in AlGaIn/GaN HEMTs result in larger 2DEG densities. Such a trend can be explained as due to improved carrier confinement. The slope of the n_s - V_{gs} plots corresponds to the gate capacitance. As is found, this capacitance is more sensitive to the AlGaIn layer thickness as compared to Al composition. On the other hand, to examine the relation between the sheet concentration of 2DEG and the doping content, we computed the density n_s as a function of N_D for parameters x and d_d fixed at 0.22 and 28 nm. Two peculiar features were revealed: (i) the 2DEG density increases with doping concentration and (ii) the sensitivity of sheet charge to the AlGaIn barrier thickness is greater at

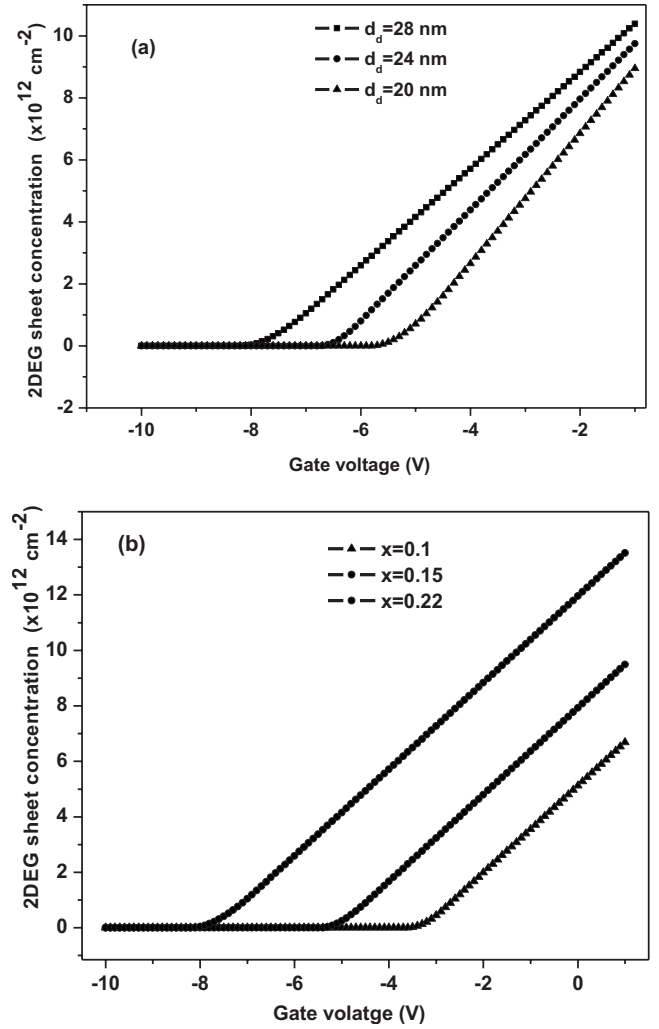


FIG. 2. The 2D sheet charge density in an AlGaIn/GaN HEMT as calculated vs the gate bias for different AlGaIn layer thicknesses (a) and Al compositions (b).

higher doping contents. It has to be noticed that larger d_d and smaller N_D are more convenient, since both give lower gate capacitance and reduced effects of deep traps related to donors.

Based on this model for evaluating the 2DEG sheet density, our interest has also been focused on the electron transport in operating AlGaIn/GaN HEMTs. To this end, we have the drain current using Eqs. (9) and (10). Figure 3 shows the current-voltage characteristics for different values of gate bias, as calculated for an AlGaIn/GaN heterostructure with $x = 0.22$, $d_i = 3 \text{ nm}$, $d_d = 28 \text{ nm}$, $L = 0.3 \text{ } \mu\text{m}$, $Z = 100 \text{ } \mu\text{m}$, $N_D = 10^{18} \text{ cm}^{-3}$, $T = 300 \text{ K}$, $R_s = 0.5 \text{ } \Omega \text{ mm}$ and $R_d = 0.5 \text{ } \Omega \text{ mm}$. As shown from the characteristics, the saturated drain current increases with increased gate voltage. In the inset of Fig. 3, is reported the variation of saturated drain current as a function of doping density at different Al compositions. The plots reveal enhanced drain current in increasing the doping density and the Al mole fraction. It should be, however, noted that the use of weaker doping concentrations and high Al contents seem to be an appropriate way to achieve improved electron transport in AlGaIn-related HEMTs. Additionally, to assess the microwave performance

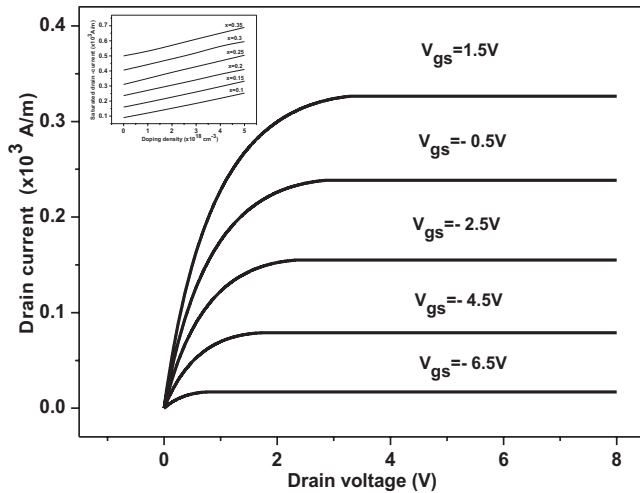


FIG. 3. Calculated V_{ds} - I_{ds} characteristics for an AlGaIn/GaN HEMT at different gate voltages. The inset shows the dependence of the dc drain current as a function of the doping content for different Al compositions.

of a high-power transistor device, the transconductance and gate conductance have to be analyzed and optimized. For the AlGaIn/GaN heterostructures to modelize, these parameters have been evaluated versus the fundamental device parameters and applied bias voltages. Concerning the transconductance, the results obtained are: (i) higher transconductances are expected to be attained at lower gate lengths and at smaller barrier widths as well and (ii) at relatively high Al compositions, the peak transconductance is found to be occurring at lower gate voltages. High values of transconductance in GaN-based HEMTs are assigned to high carrier density due to strong polarization effects. As demonstrated above, decreasing the thickness of AlGaIn/GaN barrier is recommended to achieve a high transconductance. However this leads to a decrease in both the total amount of donor atoms and the 2DEG sheet concentration. To overcome this limitation, the employment of a delta-doping instead of bulk doping in the AlGaIn barrier epilayer would most probably give higher sheet concentrations of 2DEG with a high transconductance. For the drain conductance, however, calculations led to the following observations (i) the drain conductance decreases with the increasing of in drain voltage and increases with the gate bias, (ii) as the Al mole fraction is increased, the drain conductance increases and is higher at smaller gate lengths. As evidenced from the latter study, the use of higher Al contents with relatively thin gates is essential to further improve the microwave performance of designed AlGaIn/GaN HEMTs.

C. The self-heating in AlGaIn/GaN HEMTs

As established for GaN-based HEMTs, the AlGaIn/GaN band offset and spontaneous and piezoelectric polarization fields occurring in the heterostructure create a quasi-2DEG with relatively high free-carrier concentrations located in GaN at the interface with AlGaIn. Because the drain current is subjected to flow in the 2DEG conductive channel, collisional energy loss from electrons to the crystal lattice leads to a local heating. Two main processes govern the heat dissipation in operating AlGaIn/GaN HEMTs: ionized defect

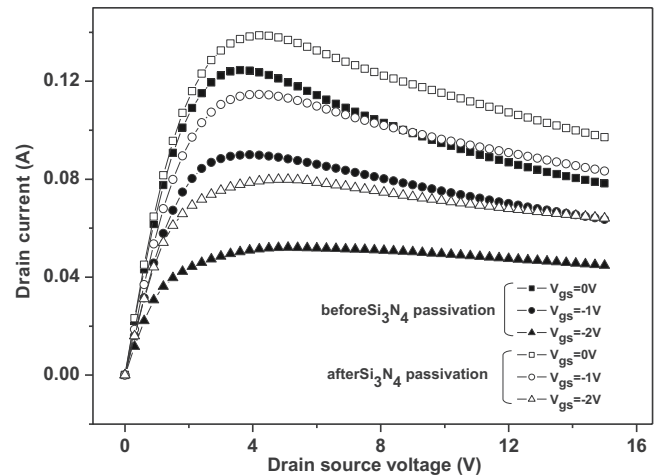


FIG. 4. Output characteristics of AlGaIn/GaN/SiC HEMTs before and after Si_3N_4 passivation at different gate voltages.

scattering and electron-phonon interaction. In polar semiconductors such as GaN and AlN and their alloys, the electron energy loss is primarily caused by the electron-phonon mechanism. Due to the self-heating, the temperature profile along the depth of the active epilayers is not homogeneous and shows a z -dependent rise, $\Delta T(z)$, with respect to that in equilibrium. On the other hand, the substrate has an important role in evacuating the heat generated. Improving the heat dissipation may be accomplished by using a substrate of higher thermal conductivity. SiC substrates, indeed, offer improved heat sinking into the channel and an efficient heat removal through thermal contacts deposited on the top of the HEMT devices. More accurately, to include thermal effects resulting from the self-heating in calculating the output current-voltage, the dependence of band offset, polarization fields, and electron mobility on temperature should be accounted for. Here, these parameters were defined with their temperature dependence. Figure 4 shows the drain-source current versus drain voltage investigated in our laboratory at room temperature on a AlGaIn/GaN/SiC HEMT with Al composition $x=0.22$ and for a $140 \times 0.25 \mu\text{m}^2$ gate. Measurements have been performed at $V_{gs}=0$ V. It is apparent that the saturation current exhibits a negative conductance at large V_{ds} . The decrease in current at higher drain-source voltage is due to the self-heating and especially results in a decrease in electron mobility. From experimental V_{ds} - I_{ds} data, we deduced the temperature rise of the 2DEG. The procedure adopted consists in determining T such as $I_{ds}^{\text{exp.}} - I_{ds}^{\text{th.}} = 0$ for fixed drain-voltage. In solving this equation, we considered the normalized current characteristics relative to that at room temperature. The results are illustrated in Fig. 5(a). As can be seen, the temperature rise increases with increased drain-voltage in the 4–15 V range. In a second step, we investigated the effect of the gate-bias V_{gs} on the temperature rise ΔT . As has been found, ΔT shows an increasing trend as V_{gs} increases, see Fig. 5(a). The latter behavior can be explained as resulting from the increasing of the electron sheet density in the channel. The built-in electric field at the gate-source

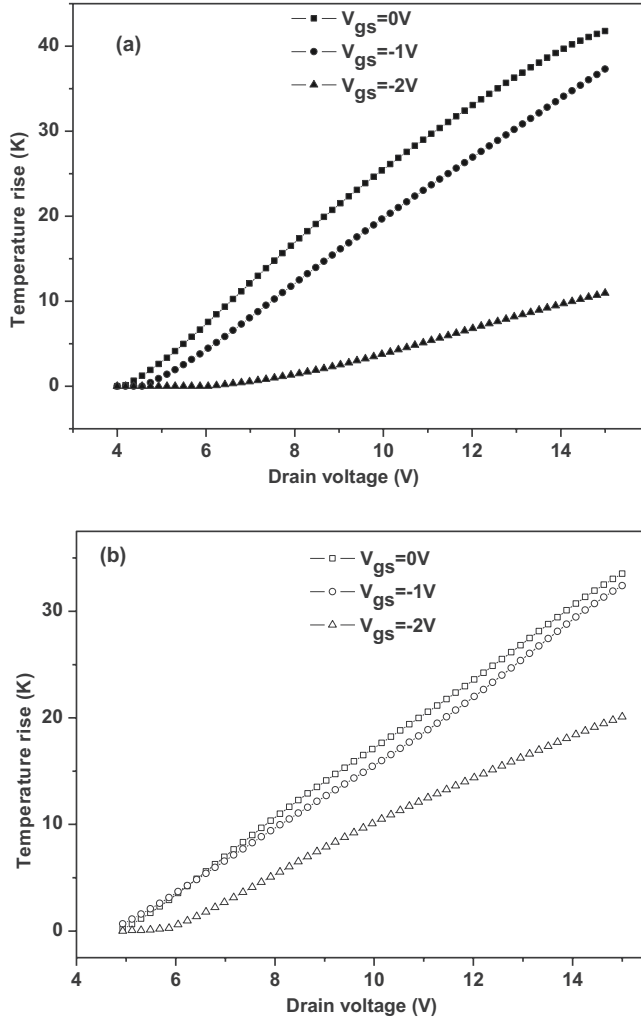


FIG. 5. Temperature rise of the 2DEG in AlGaIn/GaN/SiC HEMTs vs drain voltage at different gate biases before (a) and after (b) Si_3N_4 passivation.

heterojunction also causes an increase in $V_{gs}-I_{ds}$. Using polynomial laws we fitted the V_{ds} -dependence of the temperature rise. Obtained analytical expressions are summarized in Table I. In addition to self-heating, deep traps are also present in the AlGaIn/GaN heterostructure and can reduce the microwave performance of designed HEMTs. Such trapping effects occur both at the surface and in bulk of the GaN epilayer. Opposite to bulk defects, the number as well as the activity of surface trapping centers would be partly mitigated during process by using an appropriate passivation. As candidates, SiO_2 , MgO , AlN , and Si_3N_4 can be used to passivate

GaN-based HEMTs.^{52–55} Much higher gate current has been, however, found for Si_3N_4 passivation.⁵⁵ In the present work, we investigated the self-heating in an AlGaIn/GaN HEMT with Al composition $x=0.22$ before Si_3N_4 passivation. Obtained dc characteristics at $T=300$ K are reported in Fig. 4. Measurements were performed at $V_{gs}=0, -1$ and -2 V, respectively. As clearly seen, for all the gate biases studied, improvements in drain current are achieved after passivation with Si_3N_4 . The reason for enhanced electron transport is the increase in sheet carrier concentration. This is mainly due to the reduction in surface states. As for AlGaIn/GaN HEMTs before passivation, the self-heating is also observed in dc characteristics after Si_3N_4 passivation. We calculated the temperature rise ΔT in the 2DEG channel versus V_{ds} for different V_{gs} , Fig. 5(b). The plots reveal similar increasing tendency of $V_{ds}-\Delta T$. In Table I, also reported are the fitting laws of $V_{gs}-\Delta T$ as obtained for AlGaIn/GaN HEMTs after Si_3N_4 passivation. It is worth noticing that the local temperature in the 2DEG channel does not exhibit a significant change, compared to that in AlGaIn-related HEMTs before Si_3N_4 passivation.

III. CONCLUSION

Direct-current characteristics of AlGaIn/GaN HEMTs have been calculated from self-consistent solutions of Schrodinger and Poisson equations. The effects of temperature on the polarization and conduction-band discontinuity at the AlGaIn/GaN heterointerface have been taken into account in the modeling. The numerical simulation has been made at first without considering the self-heating and trapping effects. As the main result, AlGaIn/GaN HEMTs with higher Al composition are expected to show enhanced saturation current when compared with the same doping concentration. A charge control model based on a self-consistent analysis is also reported to investigate the influence of thermal effects on the drain-source current. For this purpose, we developed a numerical method to evaluate the temperature rise in the 2DEG conductive channel. As an experimental support, we used dc characteristics obtained at room temperature on AlGaIn/GaN HEMTs grown on SiC substrate. As is found, the temperature rise depends on the bias voltages and does not exceed 40 K. On the other hand, we studied the electron transport in AlGaIn/GaN/SiC HEMTs before Si_3N_4 passivation. As a result, the output drain current is seen to exhibit an increasing tendency with passivation. The self-heating is observed in AlGaIn/GaN HEMTs after Si_3N_4 passivation as well.

TABLE I. The fit of the 2DEG temperature rise vs drain voltage as obtained for AlGaIn/GaN/SiC HEMTs before and after Si_3N_4 passivation.

V_{gs} (V)	2 DEG Temperature rise ΔT (K)	
	Before Si_3N_4 passivation	After Si_3N_4 passivation
0	$6.49 - 8.46V_{ds} + 2.27(V_{ds})^2 + 0.165(V_{ds})^3 + 0.004(V_{ds})^4$	$-17.3 + 3.55V_{ds} - 0.01(V_{ds})^2$
-1	$21.9 - 14.6V_{ds} + 3.03(V_{ds})^2 - 0.21(V_{ds})^3 + 0.005(V_{ds})^4$	$-11.5 + 2.25V_{ds} + 4.95(V_{ds})^2$
-2	$4.08 - 1.5V_{ds} + 0.09(V_{ds})^2 - 0.011(V_{ds})^3 - 0.0006(V_{ds})^4$	$32.3 - 17V_{ds} + 2.96(V_{ds})^2 - 0.19(V_{ds})^3 + 0.0045(V_{ds})^4$

- ¹R. Gaska, M. S. Shur, A. D. Bykhovski, A. O. Orlov, and G. L. Snider, *Appl. Phys. Lett.* **74**, 287 (1999).
- ²M. A. Khan, Q. Chen, M. S. Shur, B. T. McDermott, and J. A. Higgins, *IEEE Electron Device Lett.* **17**, 325 (1996).
- ³R. Dimitrov, L. Wittmer, H. P. Felsl, A. Mitchell, O. Ambacher, and M. Stutzmann, *Phys. Status Solidi A* **168**, R7 (1998).
- ⁴Q. Chen, J. W. Yang, R. Gaska, M. A. Khan, M. S. Shur, G. J. Sullivan, A. L. Sailor, J. A. Higgins, A. T. Ping, and I. Adesida, *IEEE Electron Device Lett.* **19**, 44 (1998).
- ⁵Y. F. Wu, B. P. Keller, P. Fini, S. Keller, T. J. Jenkins, L. T. Kehias, S. P. Denbaars, and U. K. Mishra, *IEEE Electron Device Lett.* **19**, 50 (1998).
- ⁶A. T. Ping, Q. Chen, J. W. Yang, M. A. Khan, and I. Adesida, *IEEE Electron Device Lett.* **19**, 54 (1998).
- ⁷S. J. Pearton, J. C. Zopler, and F. Ren, *J. Appl. Phys.* **86**, 1 (1999).
- ⁸R. Gaska, Q. Chen, J. Yang, A. Osinsky, M. A. Khan, and M. S. Shur, *IEEE Electron Device Lett.* **18**, 492 (1997).
- ⁹N. Maeda, K. Tsubaki, T. Saitoh, T. Tawara, and N. Kobayashi, *Appl. Phys. Lett.* **79**, 1634 (2001).
- ¹⁰N. Maeda, T. Saitoh, K. Tsubaki, T. Nishida, and N. Kobayashi, *Mater. Sci. Eng., B* **82**, 232 (2001).
- ¹¹N. Maeda, T. Nishida, N. Kobayashi, and M. Tomizawa, *Appl. Phys. Lett.* **73**, 1856 (1998).
- ¹²J. Antoszewski, M. Gracey, J. M. Dell, L. Faraone, T. A. Fisher, G. Parish, Y.-F. Wu, and U. K. Mishra, *J. Appl. Phys.* **87**, 3900 (2000).
- ¹³Y. Zhang, I. P. Smorchkova, C. R. Elsass, S. Keller, J. P. Ibbeston, S. Denbaars, U. K. Mishra, and J. Singh, *J. Appl. Phys.* **87**, 7981 (2000).
- ¹⁴J. P. Ibbeston, P. T. Fini, K. D. Ness, S. P. DenBaars, J. S. Speck, and U. K. Mishra, *Appl. Phys. Lett.* **77**, 250 (2000).
- ¹⁵S. L. Rumyantsev, N. Pala, M. S. Shur, R. Gaska, M. E. Levinshtein, M. A. Khan, G. Simin, X. Hu, and J. Yang, *J. Appl. Phys.* **88**, 6726 (2000).
- ¹⁶C. P. Jiang, S. L. Guo, Z. M. Huang, J. Yu, Y. S. Gui, G. Z. Zheng, J. H. Chu, Z. W. Zheng, B. Shen, and Y. D. Zheng, *Appl. Phys. Lett.* **79**, 374 (2001).
- ¹⁷F. Bernardini, V. Fiorentini, and D. Vanderbilt, *Phys. Rev. B* **56**, R10024 (1997).
- ¹⁸A. Zoroddu, F. Bernardini, P. Ruggerone, and V. Fiorentini, *Phys. Rev. B* **64**, 045208 (2001).
- ¹⁹O. Ambacher, B. Foutz, J. Smart, J. R. Shealy, N. G. Weimann, K. Chu, M. Murphy, A. J. Sierakowski, W. J. Schaff, L. F. Eastman, R. Dimitrov, A. Mitchell, and M. Stutzmann, *J. Appl. Phys.* **87**, 334 (2000).
- ²⁰V. Fiorentini, F. Bernardini, and O. Ambacher, *Appl. Phys. Lett.* **80**, 1204 (2002).
- ²¹N. Maeda, K. Tsubaki, T. Saitoh, T. Tawara, and N. Kobayashi, *Opt. Mater. (Amsterdam, Neth.)* **23**, 211 (2003).
- ²²I. Saidi, L. Bouzaïene, M. H. Gazzah, H. Mejri, and H. Maaref, *Solid State Commun.* **140**, 308 (2006).
- ²³K. Horio and A. Nakajima, *Phys. Status Solidi C* **5**, 1898 (2008).
- ²⁴R. Vetry, N. Q. Zhang, S. Keller, and U. K. Mishra, *IEEE Trans. Electron Devices* **48**, 560 (2001).
- ²⁵P. B. Klein, *J. Appl. Phys.* **92**, 5498 (2002).
- ²⁶S. Arulkumaran, T. Egawa, H. Ishikawa, and T. Jimbo, *Appl. Phys. Lett.* **81**, 3073 (2002).
- ²⁷A. P. Zhang, L. B. Rowland, E. B. Kaminsky, V. Tilak, J. C. Grande, J. Teetsov, A. Vertiatchikh, and L. F. Eastman, *J. Electron. Mater.* **32**, 388 (2003).
- ²⁸M. Gassoumi, J. M. Bluet, C. Gaquière, G. Guillot, and H. Maaref, *Mater. Sci. Eng., C* **28**, 787 (2008).
- ²⁹M. Asif Khan, A. Bhattarai, J. N. Kuznia, and D. T. Olson, *Appl. Phys. Lett.* **63**, 1214 (1993).
- ³⁰M. A. Khan, X. Hu, A. Tarakji, G. Simin, J. Yang, R. Gaska, and M. Shur, *Appl. Phys. Lett.* **77**, 1339 (2000).
- ³¹M. E. Levinshtein, S. L. Rumyantsev, and M. Shur, *Properties of Advanced Semiconductor Materials* (Wiley, New York, 2001).
- ³²J. Zou, D. Kotchetkov, A. A. Balandin, D. I. Florescu, and F. H. Pollak, *J. Appl. Phys.* **92**, 2534 (2002).
- ³³R. Gaska, A. Osinsky, J. W. Yang, and M. S. Shur, *IEEE Electron Device Lett.* **19**, 89 (1998).
- ³⁴I. Ahmad, V. Kasisomayajula, M. Holtz, J. M. Berg, S. R. Kurtz, C. P. Tigges, A. A. Allerman, and A. G. Baca, *Appl. Phys. Lett.* **86**, 173503 (2005).
- ³⁵I. Ahmad, V. Kasisomayajula, D. Y. Song, L. Tian, J. M. Berg, and M. Holtz, *J. Appl. Phys.* **100**, 113718 (2006).
- ³⁶J. Kim, J. A. Freitas, Jr., J. Mittereder, R. Fitch, B. S. Kang, S. J. Pearton, and F. Ren, *Solid-State Electron.* **50**, 408 (2006).
- ³⁷J. D. Albrecht, P. P. Ruden, S. C. Binari, and M. G. Ancona, *IEEE Trans. Electron Devices* **47**, 2031 (2000).
- ³⁸A. Asgari, M. Kalafi, and L. Faraone, *Phys. Status Solidi C* **2**, 1047 (2005).
- ³⁹Y. Chang, Y. Zhang, Y. Zhang, and Y. Tong, *J. Appl. Phys.* **99**, 044501 (2006).
- ⁴⁰M. K. Chattopadhyay and S. Tokekar, *Microelectron. J.* **39**, 1181 (2008).
- ⁴¹E. W. Faraclas and A. F. M. Anwar, *Solid-State Electron.* **50**, 1051 (2006).
- ⁴²Y. Chang, Y. Tong, and C. Surya, *Semicond. Sci. Technol.* **20**, 188 (2005).
- ⁴³A. B. Jazia, H. Mejri, H. Maaref, and K. Souissi, *Semicond. Sci. Technol.* **12**, 1388 (1997).
- ⁴⁴R. M. Chu, Y. D. Zheng, Y. G. Zhou, S. L. Gu, B. Shen, and R. Zhang, *Opt. Mater. (Amsterdam, Neth.)* **23**, 207 (2003).
- ⁴⁵Rashmi, A. Kranti, S. Haldar, and R. S. Gupta, *Solid-State Electron.* **46**, 621 (2002).
- ⁴⁶Rashmi, A. Kranti, S. Haldar, and R. S. Gupta, *Microelectron. J.* **33**, 205 (2002).
- ⁴⁷Rashmi, A. Kranti, S. Haldar, M. Gupta, and R. S. Gupta, *IEEE Trans. Microwave Theory Tech.* **51**, 607 (2003).
- ⁴⁸P. Tripathi and B. K. Ridley, *Phys. Rev. B* **66**, 195301 (2002).
- ⁴⁹D. Zanato, S. Gokden, N. Balkan, B. K. Ridley, and W. J. Schaff, *Semicond. Sci. Technol.* **19**, 427 (2004).
- ⁵⁰S. Gokden, A. Ilgaz, N. Balkan, and S. Mazzucato, *Physica E* **25**, 86 (2004).
- ⁵¹D. Zanato, S. Gokden, N. Balkan, B. K. Ridley, and W. J. Schaff, *Superlattices Microstruct.* **34**, 77 (2003).
- ⁵²W. S. Tan, P. A. Houston, P. J. Parbrook, G. Hil, and R. J. Airey, *J. Phys. D* **35**, 595 (2002).
- ⁵³X. Z. Dang, E. T. Yu, E. J. Piner, and B. T. McDermott, *J. Appl. Phys.* **90**, 1357 (2001).
- ⁵⁴W. Lu, V. Kumar, R. Schwindt, E. Piner, and I. Adesida, *Solid-State Electron.* **46**, 1441 (2002).
- ⁵⁵J. Bernát, P. Javorka, A. Fox, M. Marso, H. Lüth, and P. Kordoš, *Solid-State Electron.* **47**, 2097 (2003).